

Energy landscape of silicon systems and its description by force fields, tight binding schemes, density functional methods, and quantum Monte Carlo methods

S. Alireza Ghasemi,¹ Maximilian Amsler,¹ Richard G. Hennig,² Shantanu Roy,¹ Stefan Goedecker,^{1,*} Thomas J. Lenosky,³ C. J. Umrigar,⁴ Luigi Genovese,⁵ Tetsuya Morishita,⁶ and Kengo Nishio⁶

¹*Department of Physics, Universität Basel, Klingelbergstr. 82, 4056 Basel, Switzerland*

²*Department of Materials Science and Engineering, Cornell University, Ithaca, New York 14850, USA*

³*C8 Medisensors, Los Gatos, California 95032, USA*

⁴*Laboratory of Atomic and Solid State Physics, Cornell University, Ithaca, New York 14853, USA*

⁵*European Synchrotron Radiation Facility, 6 rue Horowitz, 38043 Grenoble, France*

⁶*Research Institute for Computational Sciences (RICS), National Institute of Advanced Industrial Science and Technology (AIST), 1-1-1 Umezono, Tsukuba, Ibaraki 305-8568, Japan*

(Received 20 October 2009; revised manuscript received 23 April 2010; published 9 June 2010)

The accuracy of the fundamental properties of the energy landscape of silicon systems obtained from density functional theory with various exchange-correlation functionals, a tight binding scheme, and force fields is studied. Depending on the application, quantum Monte Carlo or density functional theory results serve as quasixact reference values. In addition to the well-known accuracy of density functional methods for geometric ground states and metastable configurations we find that density functional methods give a similar accuracy for transition states and thus a good overall description of the energy landscape of the silicon systems. On the other hand, force fields give a very poor description of the landscape that are in most cases too rough and contain many spurious local minima and saddle points or ones that have the wrong height.

DOI: [10.1103/PhysRevB.81.214107](https://doi.org/10.1103/PhysRevB.81.214107)

PACS number(s): 61.46.Df, 31.15.A–

I. INTRODUCTION

In spite of the great progress in density functional theory (DFT) for treating large systems, it is at present not possible to treat systems with more than about 1000 atoms in complex simulations where forces and energies have to be evaluated many times. This is, for instance, necessary in molecular dynamics simulations where one has to follow the evolution of the system over long time intervals or in global optimization methods for finding the ground-state geometry. In these kinds of situations faster and more approximate methods such as force fields or tight binding (TB) schemes are widely used. Because of its technological importance several widely used force fields exist for silicon and large scale simulations, which are not feasible with density functional methods, are frequently performed using these more approximate methods.

These force fields are typically fitted to a data set of ground-state structures, usually containing crystalline structures and sometimes also nonperiodic structures. An accurate description of some ground-state geometries is, however, not sufficient to ensure accurate dynamical simulations. Dynamical properties such as diffusion coefficients are related to other fundamental properties of the energy landscape such as barrier heights. The distribution of barrier heights and other fundamental properties of the silicon potential-energy surface (PES) have been studied using forcefields.¹ In a great number of publications, the accuracy of DFT calculations for structure predictions (i.e., minima on PES) for different systems as well as for silicon, has been studied and compared with both high-level quantum-mechanical approaches^{2–4} and experimental data.^{5,6} In this paper we study overall fundamental properties of the energy landscape which are relevant in many different contexts. We look, in particular, at the ac-

curacy of the barrier heights in the various schemes used for large scale simulations of silicon systems. Since it is known that the barrier heights relevant to chemical reactions are not very well described with standard density functionals such as local-density approximation (LDA) (Ref. 7) or Perdew-Burke-Ernzerhof (PBE),⁸ we benchmark some of the energy barriers using accurate quantum Monte Carlo (QMC) methods. There are two forms of QMC methods that are used for electronic-structure calculations, the simpler variational MC (Ref. 9) (VMC) and the more sophisticated diffusion MC (Refs. 10 and 11) (DMC). In VMC, quantum-mechanical expectation values are calculated using Monte Carlo techniques to evaluate the many-dimensional integrals. The accuracy of the results depends crucially on the quality of the trial wave function. The DMC removes most of the error in the trial wave function. DMC is a stochastic projector method that projects out the ground state from the trial wave function using an integral form of the imaginary-time Schrödinger equation. For fermionic systems, the antisymmetry constraint leads to the fermion-sign problem that is cured by fixing the nodes of the projected state to be those of an approximate trial wave function. The resulting fixed-node error is the main uncontrolled error in DMC. Currently, a systematic improvement of the wave function by optimization of an increasing number of variational parameters is the most practical approach for reducing the fixed-node error.^{12–14} A good description of quantum Monte Carlo methods used in physics and chemistry can be found in Refs. 15–17.

Force fields and other approximate methods are sometimes applied to systems that are very different from the systems that were in the fitting database. The question is therefore how reliable are force-field-based structure predictions of complex structures such as defects, interfaces, or clusters. In most studies of such systems only one force field

was used but in some exceptionally careful studies, such as in the study of dislocation kinks in silicon¹⁸ and a comparative study of silicon empirical interatomic potentials,¹⁹ the results of several force fields were compared and significant discrepancies in the results obtained from different force fields were indeed found.

Balamane *et al.*¹⁹ performed an extensive study on comparison of different silicon force fields for clusters, surfaces, and crystalline structures. They found that the employed force fields are sufficiently accurate only for diamond structure and its intrinsic defects and among surfaces only for Si(001). In addition they found that all force fields were unable to predict the equilibrium structures of small Si clusters. Samela *et al.*²⁰ compared three common silicon force fields for molecular-dynamics simulations of cluster bombardment of silicon structures. They concluded that while the force fields give almost similar overall description of collision cascades at different energies, measurable quantities like sputtering yields and crater sizes vary considerably between the force fields. Erkoç and Takahashi²¹ compared 15 different empirical force fields for silicon microclusters and obtained the same results as Balamane but with a greater number of trial potentials and fewer small test clusters. A comparative study of empirical potentials of silicon with emphasis on finite-temperature simulations of the Si(001) surface was presented by Nurminen *et al.*²² Their results showed the inadequacy of the force fields for surfaces similar to what Balamane *et al.* found. In addition, simulations at finite temperatures can be problematic even if the potential gives good results for zero-temperature calculations. Hensel *et al.*²³ performed a comparative study between classical and tight binding molecular dynamics for silicon growth of a reconstructed (100)-silicon crystal. They argued that accurate methods such as tight binding are needed for applications other than the crystalline diamond structure.

Since we have a variety of objectives for our paper, we summarize them as follows. Activation energies associated with transition states play an essential role in determination of the rate of thermally activated processes. Since currently DFT calculations are the most commonly used approach to predict these barrier heights, we assess the performance of various DFT exchange-correlation (XC) functionals using DMC to calculate reference values. Furthermore, we consider the energy and geometry of the low-lying configurations which are local minima of the potential energy. The analysis given addresses clusters and bulk silicon systems, general enough to suggest that the approach and conclusions may be relevant to other silicon systems. Finally, to shed light on the accuracy of force fields we examine the configurational density of states obtained by various approximate schemes for silicon. If the configurational density of states was to be independent of the method used to generate them this would be consistent with accurate local minima in the PES. Consequently we examine the differences between such quantities for a range of force fields. Consequently the density of configurations per energy interval would be identical for approximate and accurate methods.

The structure of our paper is as follows. In Sec. II, we briefly discuss the methods and computational details of our calculations. Then, in Sec. III, different DFT XC functionals

and tight binding are compared with DMC for a set of transition states and their associated minima. For all other sections of the paper, DFT (with LDA XC functional) is used to generate reference values. In Secs. IV and V, various classical potentials and tight binding are compared with each other, and whenever possible, with DFT. In Sec. IV, the topography of the PES as well as stable and metastable structures of small silicon clusters are studied. Furthermore, an unusual flatness of the DFT energy landscape in some regions is investigated in detail. Finally, in Sec. V, point defects and configurational density of states of bulk silicon are considered. Section VI presents discussions about the results and the conclusions are summarized in Sec. VII.

II. METHODS

In our study we have included the most common force fields for silicon, namely, the Tersoff force field,²⁴ the Stillinger-Weber (SW) force field,²⁵ the environmental-dependent interaction potential (EDIP) force field²⁶ and the Lenosky modified embedded-atom method (MEAM) potential.^{27,28} We also present some limited results on a re-fitted version of the Lenosky force field, labeled as reparameterized Lenosky force field, which has the same functional form and radial cutoffs but different spline parameters.²⁹ This model was specifically optimized to accurately model multiple-interstitial defect structures in silicon and was applied successfully in another paper.³⁰ The Tersoff force field was smoothly extrapolated to zero by a third-order polynomial using cut-off radii that are large enough to ensure a smooth behavior of the potential. The cut-off values were 2.7 and 3.3 Å, where the smaller value denotes the radius where the polynomial takes over and the larger value the radius where the polynomial interaction drops to zero.

The Lenosky TB (Ref. 31) (LTB) scheme was chosen to provide a scheme considered to be intermediate in computational cost and accuracy between *ab initio* approaches and force fields. We employed Kohn-Sham DFT using three categories of exchange-correlation functionals, i.e., local-density approximation, generalized gradient approximation, and hybrid functionals. Apart from the preparation of trial wave function for QMC calculations and DFT barrier heights within B3LYP,³² all other DFT calculations are performed with the BigDFT (Ref. 33) package, a pseudopotential-based^{34,35} DFT code with a wavelet basis set. Wavelets are a systematically extendable basis set and the basis size was chosen sufficiently large that energies were converged to better than to 0.01 eV. In all geometry optimizations [for both cases saddle points (SPs) and minima] the force-maximum component on the atoms was brought down to less than 0.02 eV/Å. All DFT calculations were performed at Γ -point. Grid spacing of 0.21 Å is used in all BigDFT calculations. The number of grid points determines the number of basis functions used in the calculation.

The QMC calculations are performed using the CHAMP code developed by Umrigar, Filippi, and Toulouse. The 1s, 2s, and 2p electrons of Si are eliminated using a Hartree-Fock pseudopotential.³⁶ The trial wave function consists of a sum of Slater determinants of single-particle orbitals multi-

plied by a Jastrow factor. The orbitals of the Slater determinant are taken from a DFT calculation using GAMESS (Refs. 37 and 38) with the B3LYP (Ref. 32) exchange-correlation functional. The excitations included in the sum of Slater determinants are those with the largest weights in a configuration interaction with single and double excitation (CISD) calculations. Configuration state functions (CSFs), i.e., linear combinations of determinants that have the correct spatial and spin symmetries, are used to reduce the number of variational parameters. The Jastrow correlation function describes electron-electron, electron-nuclear, and electron-electron nuclear correlations. The Jastrow parameters and the CSF coefficients are optimized in VMC using a recently developed energy minimization method.¹²⁻¹⁴ Finally, DMC calculations using the optimized trial wave function and a time step of 3.7×10^{-4} eV⁻¹ determine the energies of the structures. Most of the calculations employed a single determinant, but to estimate the size of the fixed-node error we performed, for some structures, VMC and DMC calculations with trial wave functions containing an increasing number of Slater determinants up to 150.

III. TRANSITION STATES OF Si₈

According to transition-state theory, the height and the shape of saddle points and their associated minima determine, in an approximate manner, the dynamical behavior of a system.³⁹ Some efforts have been made by prior authors to assess the effect of approximate-energy landscapes on the dynamics of silicon systems, however, the overall picture remains unclear.⁴⁰⁻⁴² In order to investigate the quality of the silicon potential-energy landscape within various schemes we performed simulations to find saddle points of small Si₈ clusters using DFT within the local-density approximation. We then compared the barrier heights for these LDA configurations with the heights obtained from other XC functionals, namely, with a generalized gradient approximation functional (PBE), a hybrid functional (B3LYP), and accurate QMC methods. The eight-atom silicon cluster was chosen because for this size, QMC is computationally not too expensive. In agreement with previous work⁴³ we found that the saddle-point geometries are nearly identical within different XC functionals. The maximum displacement of an atom of a PBE saddle-point geometry is only 0.02 Å from the LDA one. This justifies the use of LDA geometries in all energy calculations. We also compared DFT saddle-point results with the Lenosky tight binding method. Previous authors have found that quantum Monte Carlo has demonstrated its ability to provide accurate reaction barrier heights. Calculated values agreed with the experimental values to within the statistical error bar of 0.07 eV⁴⁴ for some organic molecules and to within 0.005 eV (see Refs. 45 and 46) for the well-known exchange reaction $H+H_2 \rightarrow H_2+H$. We will therefore consider in the following our QMC results as accurate reference values.

To generate our saddle-point configurations, we started with the putative global minimum of the Si₈ cluster⁴⁷ and using the improved dimer method⁴⁸ we found six saddle points (SP1–SP6) which connect the putative global mini-

um state to other ones or to itself—the latter corresponds to the exchange of two silicon atoms (SP1 and SP4). Furthermore, two more saddle points (SP7 and SP8) were obtained starting from the first low-lying isomer. One of them (SP7) corresponds to the exchange of two atoms. Finding the saddle points and the adjacent minima was done within LDA using the BIGDFT (Ref. 33) package.

There are numerous publications (for a survey see Ref. 49) in which it is shown that DFT with conventional XC functionals gives poor transition-state barrier heights for chemical reactions.⁵⁰⁻⁵² Within LDA and GGA's the results are most unsatisfactory for hydrogen-transfer reactions where covalent hydrogen bonds are broken and formed. The most simple and prominent example is the exchange reaction $H+H_2 \rightarrow H_2+H$ where the conventional XC functionals do not predict a barrier at all. The poor performance seems to be due to poor cancellation of the electrostatic self-interaction errors in the conventional XC functionals.⁵³ In the literature this problem is known as “self-interaction error” which is related to the delocalization error.⁵⁴ Hybrid functionals, which give a better error cancellation, give an improved barrier height in this case.⁴⁹ Nevertheless researchers usually resort to wave-function methods if highly accurate barrier heights are needed for chemical reactions.

Table I shows that in our case the situation is entirely different. Figure 1 illustrates the correlations LDA, PBE, and B3LYP barrier heights with respect to DMC results. As already noted above, DMC calculations provide our standard of accuracy. The root-mean-square (rms) errors for LDA, PBE, and B3LYP are 0.062 eV, 0.074 eV, and 0.159 eV, respectively. While LDA is generally regarded as a less accurate functional than PBE or B3LYP, we actually found the surprising result that it worked better than both PBE and B3LYP. How can this surprising accuracy be explained? In contrast to chemical reactions our clusters are never torn apart into fragments when they move along the minimum-energy pathway from one local minimum over a saddle point into another local minimum. Even at the transition state (see Figs. 2 and 3) the silicon atoms are all in an environment that is similar to the environment at a local minimum and one cannot distinguish a saddle-point configuration from a local minimum-energy configuration by inspection. DFT self-interaction errors⁵⁴ are therefore expected to cancel to a large degree. For similar reasons, highly inhomogeneous environments with large density gradients, which can be better treated with gradient corrected and generalized gradient functionals, are situations not relevant for our calculation. We believe these two arguments explain the unusually good performance of LDA in our barrier calculations.

B3LYP,³² being a hybrid functional, is a linear combination of local and gradient corrected exchange and correlation functionals with three adjustable parameters that were fitted to a database of cohesive energies of small molecules. Motivated by the idea of empirically fitting of an XC functional, we write

$$E_{pred} = a_1 \times E_{LDA} + a_2 \times E_{PBE} + a_3 \times E_{B3LYP}. \quad (1)$$

Instead of empirically fitting a functional, we took a weighted sum of the total energies from several methods,

TABLE I. Comparison of the barrier height (BH) energies of eight saddle-point (SP) configurations relative to the two neighboring minima calculated with various XC functionals and QMC. The saddle point and minima configurations are from LDA. The abbreviation for the various XC functionals are defined in the text. VMC and DMC stand for variational and diffusion QMC, MD-VMC and MD-DMC for multideterminant VMC and DMC. The HOMO-LUMO gaps for the minima (HLGM) and for the saddle points (HLGS) are calculated within LDA using the BigDFT code. The statistical errors are given in parentheses. All energies are in electron volts.

System	HLGM	HLGS	LDA	PBE	B3LYP	VMC	DMC	MD-VMC	MD-DMC	TB
SP1-BH1/2	1.45	0.55	0.359	0.367	0.405	0.434(23)	0.406(13)	0.329(9)	0.338(8)	-0.046
SP2-BH1	1.45	0.41	0.735	0.729	0.770	0.809(20)	0.804(18)			-0.286
SP2-BH2	0.22		0.077	0.094	0.058	0.103(22)	0.069(18)			0.166
SP3-BH1	0.96	0.64	0.043	0.050	0.056	0.046(18)	0.028(15)	0.042(9)	0.028(8)	0.201
SP3-BH2	1.45		2.900	2.689	2.328	2.927(17)	2.845(15)	2.969(8)	2.826(8)	1.934
SP4-BH1/2	1.45	0.13	1.065	1.053	1.075	1.233(18)	1.181(15)	1.131(10)	1.134(7)	0.496
SP5-BH1	1.21	0.42	0.338	0.346	0.324	0.410(18)	0.378(14)			0.398
SP5-BH2	1.45		0.766	0.761	0.800	0.883(17)	0.862(16)			0.019
SP6-BH1	1.49	0.69	0.581	0.573	0.514	0.503(18)	0.536(16)			-0.082
SP6-BH2	1.45		1.198	1.158	1.015	1.283(18)	1.194(16)			0.921
SP7-BH1/2	1.12	0.58	0.289	0.272	0.192	0.228(18)	0.224(16)			0.157
SP8-BH1	0.22	0.82	0.212	0.198	0.041	0.143(17)	0.120(16)			0.144
SP8-BH2	1.12		0.445	0.420	0.406	0.491(18)	0.445(16)			-0.264

which perhaps gives similar results. The parameters $(a_1, a_2, a_3) = (0.95, -0.59, 0.72)$ were determined by a least-squares fit of the data in Table I. The rms error obtained by this predictive equation is 0.021 eV, about 1/3 of that the LDA results. The rms error is actually similar in magnitude to the DMC error bars, and it appears likely that the fitted expression would have predictive power in other cases since the three parameters were fitted to 13 data points, a significantly greater quantity of data than the number of the fitting parameters.

Since DFT is essentially a one-determinant method one would expect that DFT results are particularly poor when transition states have multideterminant character. This is frequently the case in chemical reactions and under such circumstances multireference wave-function methods have to be employed if accurate barrier heights are needed. Small highest occupied molecular orbital (HOMO)-lowest unoccupied molecular orbital (LUMO) gaps are an indication of the importance of multireference configurations. The HOMO-

LUMO gaps of all saddle points and the adjacent minima are presented in Table I. The average HOMO-LUMO gap of saddle points is less than that of the minima by ≈ 0.65 eV. As usual the LDA and the GGA gaps are much smaller than the B3LYP gaps which are certainly more accurate. For the configurations with small HOMO-LUMO gaps we also did multideterminant QMC calculations with as many as 150 determinants. The DMC energies went down by no more than 0.05 eV. The results show that the influence of a multideterminant wave function on the barrier height is very small, in fact, introducing multideterminant wave function into QMC makes a difference of the same size as the error bars. Another indication that the multideterminant character of the saddle-point configurations can be neglected is the fact that natural occupation numbers drop rapidly from one to zero. The occupation numbers, obtained from CISD calculations using GAMESS with about 70 determinants, fall from 1.97 down to 0.04 at the HOMO-LUMO gap.

Table I also shows that the tight binding barrier heights are not reliable. Since the results are even worse for the force fields, we have not attempted to give error bars. An addi-

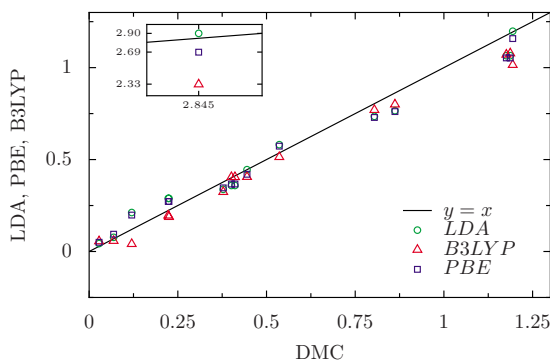


FIG. 1. (Color online) The correlation of barrier heights from DFT calculations with various XC functionals and the DMC barrier heights.

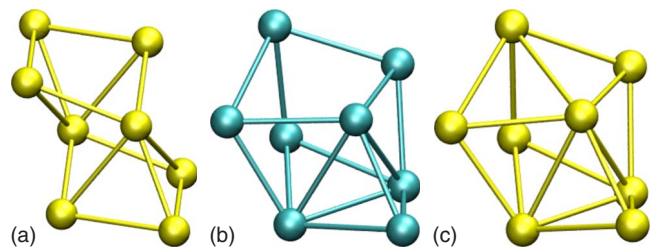


FIG. 2. (Color online) The saddle point SP2 (b) and the two neighboring minima (a), (c). It is obvious that the silicon atoms in the saddle point and the minima configurations are all in a similar environment, in particular, the saddle point is very similar to the structure (c).

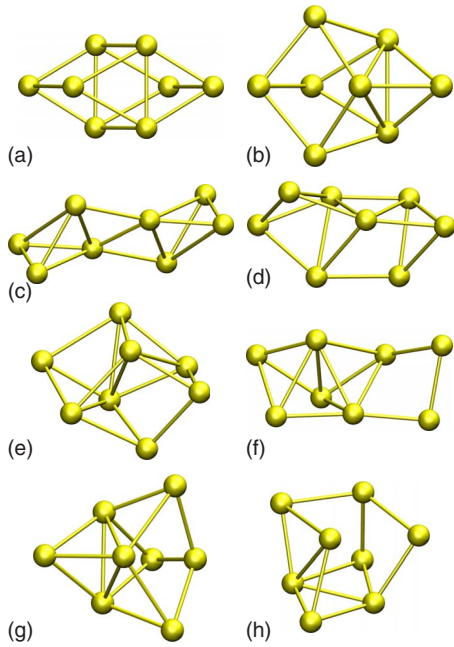


FIG. 3. (Color online) The eight Si_8 saddle points obtained by LDA calculations.

tional complication, which will be discussed in next section, is that the potential-energy surfaces of force fields contain many spurious minima and consequently also many spurious saddle points connecting the spurious minima.

IV. LOW-ENERGY CONFIGURATIONS OF SILICON CLUSTERS

A. Funnel-like structure of the PES of Si_{16}

The potential-energy surface of the Si_{16} cluster was explored systematically with all of the aforementioned classical many-body potentials and the tight binding scheme using the minima hopping method⁵⁵ (MHM). The MHM consists of a sequence of consecutive short molecular-dynamics runs and geometry relaxations. The MHM is a global optimization method which can efficiently explore the low-lying part of the energy landscape aiming at the global minimum.⁵⁶

The speed with which a system finds its ground state is evidently a physical property of the system and should carry over to most computational geometry-optimization algorithms. The efficiency also depends on the form of the corresponding potential. Systems described by potentials with staircaselike forms are possible to be relaxed efficiently to a global minimum. Hence, such systems with easily accessible ground states with well-defined structures are called structure seekers. On the other hand, potentials with a sawtooth topography lead to amorphous, glassy structures and are therefore referred to as glass formers. It is a challenging task to perform global optimization on such systems.^{57,58}

We have found considerable differences in the speed of finding the putative ground-state configuration with the MHM when using the various potentials to describe the Si_{16} cluster. Table II gives the average number n_{MIN} of minima visited before finding the putative global minimum. The dif-

TABLE II. Average values in 100 MHM runs. n_{MIN} is the number of minima visited before finding the putative ground-state configuration.

Method	n_{MIN}
EDIP	85
Lenosky	10
Reparametrized Lenosky	8
Tersoff	116
Stillinger-Weber	31
Lenosky tight binding	42
DFT	32

ferences in n_{MIN} can be ascribed to the configurational density of states (C-DOS) of the local minima for the particular potentials, discussed in Sec. V B. A large n_{MIN} indicates a high C-DOS in the low-energy region and vice versa. The Si_{16} cluster, for instance, looks more like a structure seeker with the Lenosky force field and more like a glass former with the Tersoff force field.

B. Putative ground-state and low-energy configurations of Si_{16} isomers

A database of stable configurations was generated by visiting 1000 different local minima with the MHM in each potential. To verify the accuracy of the potentials the ten energetically lowest structures were relaxed to the nearest local DFT minimum. The relaxations were performed by a simple steepest descend method with a small stepsize in the downhill direction. To increase the convergence rate a conjugate gradient method was used at the end of the relaxation. Detailed results of the investigation including geometrical properties will be discussed separately for each potential later in this section. The geometrical features to characterize surface properties of Si_{16} isomers are described in Fig. 4. In this paper the expression “excited configuration” is used for the lowest energy structures which are higher than the global minimum.

A statistical analysis was performed on the data set and the results are presented in Fig. 5 to give a quantitative in-

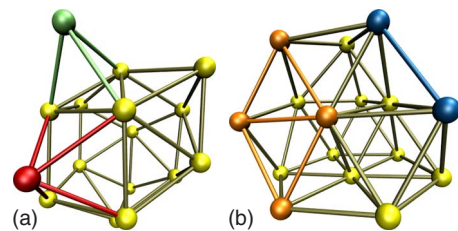


FIG. 4. (Color online) (a) A surface atom forms a sharp corner if it defines an acute-angled tetrahedral (green) or pyramidal (red) structure together with its three or four nearest neighbors, respectively. (b) Two neighboring surface atoms form a sharp edge if they make an acute-angled tetrahedral structure with the two common nearest neighbors (blue). Four neighboring surface atoms are part of a facet if they form a plane (orange).

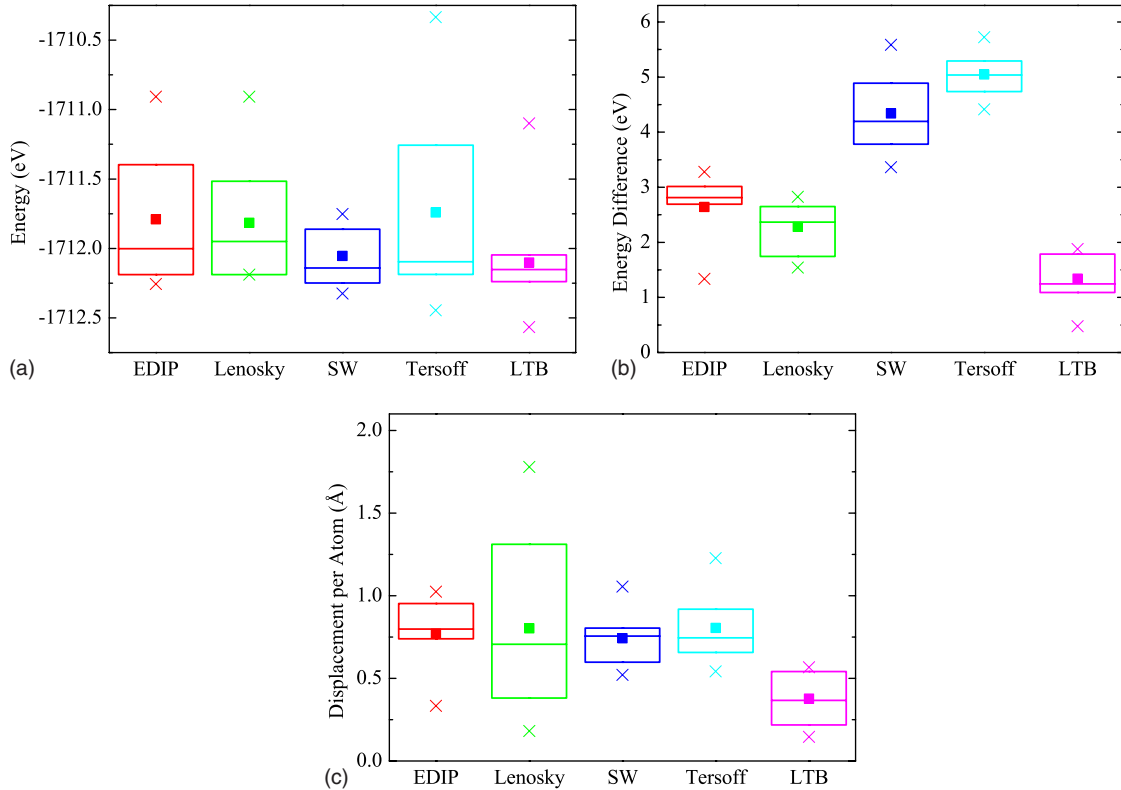


FIG. 5. (Color online) The box plots are based on ten low-lying structures of Si_{16} . The boxes contain the values ranging from the lower to the upper quartiles and the median is represented with horizontal lines. The maximum and the minimum as well as the mean values are plotted separately with crosses and squares, respectively. The absolute energy value found after relaxation in DFT are represented in (a) with arbitrary origin. Plot (b) shows the difference in DFT energy before and after relaxation. Plot (c) shows the average displacements per atom before and after relaxation. Unitary transformations of the initial and the final structures were performed to diagonalize the moment of inertia tensor with respect to each atom. The transformations which resulted in the lowest displacement were chosen. In plots (b) and (c) small values indicate better agreement of the potential with DFT results.

sight to the different characteristics of each potential. Figure 5(a) shows the energies of the low-lying configurations after relaxation in DFT. The lowest energy as well as the lowest mean energy were achieved by the LTB scheme. The small gap between the quartiles indicates a low amount of scatter. The second lowest energy was predicted by the Tersoff potential, but the scatter is considerably larger. The two other figures show how close the predicted configurations are to the nearest local DFT minimum, both energetically [Fig. 5(b)] and geometrically [Fig. 5(c)]. The SW and Tersoff force fields behave similarly. Although the median values in the relaxed energies in Fig. 5(a) are very low, the other two figures indicate a high change in energy and a moderate change in geometry during relaxation. The EDIP and Lenosky potentials perform rather moderately both in predicting energies and geometries. Only the tight binding scheme provides an overall excellent predictions of the low-lying configurations.

EDIP. The putative ground-state configuration is a hollow oblate spheroid consisting of four parallel planes. Each plane contains four atoms forming a square which are rotated by 45° with respect to the neighboring planes. The top and the bottom squares have an edge length 2.49 \AA and the intermediate planes 4.27 \AA . In this configuration all atoms are five-fold coordinated with an average bond length of 2.50 \AA . The

first nine excited configurations have the same general features as the putative ground state and only differ by forming or breaking of up to three bonds. They cover an energy range of 0.5 eV . When relaxed in DFT most of the structures are heavily deformed. In general the void regions within the structure collapse and the shape has a tendency to get elongated. Seven structures show sharp corners and edges and two structures exhibit extended facets. Only one minimum was found to be stable in DFT.

Lenosky. The third and the fourth lowest energy configurations are oblate spheroid and are the same as the second lowest and the putative global minimum configuration, respectively, of the EDIP potential. However, the putative ground-state configuration with the Lenosky potential is highly spherical consisting of four hexagonal curved panels with sixfold coordinated center atoms. Although maintaining the general form, the relaxation in DFT reveals that three of the four panels are transformed into planes. Remarkably, an excited configuration was found to relax in DFT to the above mentioned ground-state configuration (energy difference in DFT 0.7 eV). Furthermore, there are four spherical and two elongated hollow structures, only one of which is stable with DFT. All other excited states are deformed heavily and the majority show both sharp corners and edges, covering an energy range of 0.4 eV .

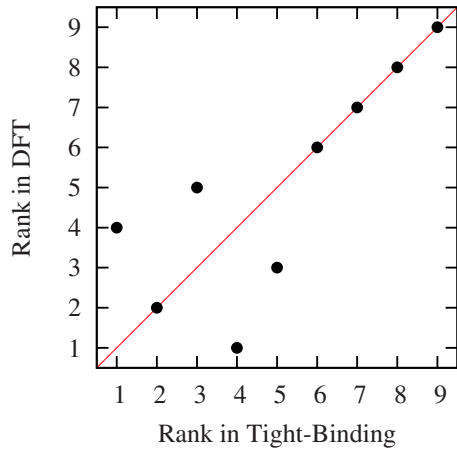


FIG. 6. (Color online) Ordering of the local minima energies in Lenosky tight binding and DFT.

Stillinger-Weber. In contrast to the previous two potentials, most configurations are highly elongated and often contain pentagonal elements. There are only three exceptions including the putative ground-state configuration which has a hollow elliptical shape formed by two square and eight pentagonal planes. Furthermore, none of the geometries contains overcoordinated atoms. The structures of all minima found with the Stillinger-Weber potential have a strong tendency to contain a large number of sharp corners and only few facets when relaxed in DFT. Although none of the structures are stable in DFT the general elongated form is often conserved and leads to low DFT energies, thus indicating an accurate description of the low-energy regions on the PES. The configurational energies are scattered over a range of 0.80 eV.

Tersoff. The putative ground-state geometry of the Tersoff potential is identical to the one found with the Stillinger-Weber potential. Only one of the nine lowest energy configurations other than the putative ground state is elongated, the other eight are very similar to the putative ground state with hollow spherical shapes. The ninth-excited state is 1.4 eV above the putative ground state. Similar to the Stillinger-Weber potential the structures do not include overcoordinated atoms. All structures are deformed after geometry optimizations with DFT and have a large number of sharp corners.

Lenosky tight binding. The Lenosky tight binding scheme predicts a putative global minimum configuration which is a slightly distorted Stillinger-Weber and Tersoff putative ground-state geometry. In contrast to the classical potentials both hollow elliptical and elongated structures without void regions are predicted in equal amounts. The energy of the ninth-excited state lies only 0.15 eV above the putative ground-state geometry, indicating an overall shallow PES. Although some bond lengths are overestimated, all structures with only one exception were found to be stable in DFT calculations. However, three configurations with similar geometries converged to the same minimum structure. The ordering of the minima with respect to the energies within the tight binding scheme and the DFT calculations is in fairly good agreement with the ideal correlation (see Fig. 6). While all four classical potentials fail to predict stable low-lying

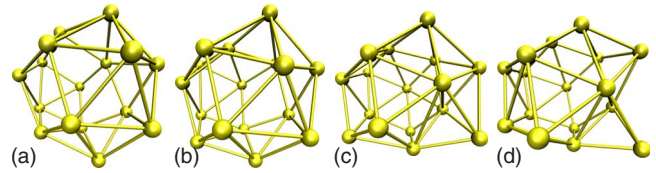


FIG. 7. (Color online) Illustration of geometry changes in a DFT relaxation of the force-field minima. (a) and (d) show the initial and the final configurations, respectively. (b) and (c) represent two snapshots of the intermediate configurations on the relaxation pathway.

Si_{16} isomers the Lenosky tight binding scheme succeeds in most cases.

In order to illustrate characteristic changes in geometries during a DFT relaxation of a force-field minimum, the initial, two intermediate, and final configurations during the relaxation of the third lowest minimum of the EDIP force field are shown in Fig. 7. This particular configuration was chosen since it has a moderate value for the average displacement per atom among all configurations relaxed in DFT, namely, ~ 0.8 Å. In Fig. 7, the formation of sharp corners can be observed while approaching the DFT minimum, a typical behavior for low-lying configurations of Si_{16} .

C. Flat regions of the PES of Si_{16} and Si_{30}

During DFT geometry relaxations of the Si_{16} one can encounter cases where the cluster is distorted considerably even though the energy decreases only slightly. Within these flat regions the norm of the force is small but may increase slightly while the monotonous downhill progress in energy is preserved. Many steps are necessary in the steepest descent DFT geometry relaxation to overcome these flat plateau regions. This behavior is discussed in the following for the DFT relaxation of the sixth lowest configuration found with the Lenosky potential. Figure 8 explicitly shows the variation in the energy with changes in geometry during the relaxation

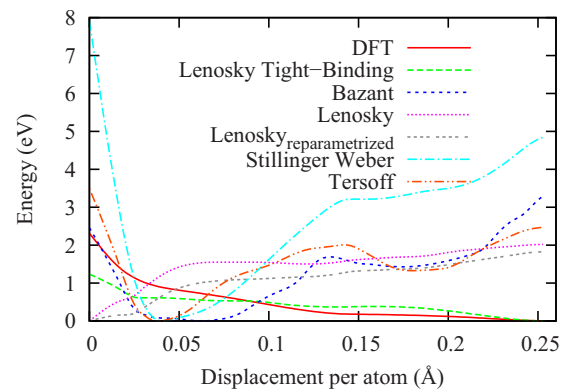


FIG. 8. (Color online) Energies of all potentials along a relaxation path in a DFT calculation plotted against the integrated atomic displacement per atom. The starting configuration is a Lenosky force field local minimum. The energies are shifted such that the minimum values are set to 0. For this calculation a tight tolerance, 0.002 eV/Å, for the maximum force component on atoms was necessary. *Lenosky_{reparametrized}* is an unpublished reparametrized Lenosky MEAM in which a single FFCD is stable (Ref. 29).

TABLE III. Statistical data related to the Hessian matrix around local minima of up to 120 random configurations of a Si₃₀ cluster. The corresponding average of largest and smallest eigenvalues of the Hessian matrices are listed (in eV/Å²). The range of the largest eigenvalues are listed in the second line. The last line contains the average condition number κ of the corresponding Hessian matrices.

	EDIP	Lenosky	SW	Tersoff	LTB	DFT
$\langle E_{large} \rangle$	61.0	43.0	38.0	58.0	23.0	27.0
$E_{large}^{max} - E_{large}^{min}$	83.0	65.0	12.0	106.0	7.0	8.0
$\langle E_{small} \rangle$	0.23	0.44	0.31	0.72	0.18	0.2
$\langle \kappa \rangle$	476.0	132.0	175.0	93.0	239.0	197.0

in the various potentials. Only the Lenosky tight binding scheme provides an accurate energy trend when following the DFT relaxation pathway. All classical potentials fail to even describe the monotonical lowering of the configurational energy along the pathway. With the exception of the Lenosky and the reparametrized Lenosky force fields they give an oscillating energy surface instead of a flat one. This is a first indication that the classical potentials give a too rough PES. Although the SW potential is smoother than EDIP and Tersoff it has a very large unphysical excursion in energy at both end points which is not the case for any of the other potentials studied. Similar performance of the various force fields was observed by Lenosky *et al.* (see Fig. 6 of Ref. 27). The MEAM ansatz of the Lenosky force field seems to give smoother potential-energy surface than the other classical potentials. Furthermore, the average number of interacting atoms were calculated for each potential along the relaxation path, but none of the potentials show a significant fluctuation from the average values. As expected, the number of interacting atoms is largest for the Lenosky tight binding, followed by both Lenosky and reparametrized Lenosky potentials. EDIP, SW, and Tersoff show a similarly low number of interacting neighbors.

The eigenvalues of the Hessian matrix were used as another quantity to describe the differences of the PES among the potentials. Since the smooth topography of the DFT Born-Oppenheimer surface should be a property fairly independent of the cluster size similar results as above can also be expected for Si₃₀ isomers. Therefore 120 random Si₃₀ configurations were relaxed using the different potentials and largest and smallest eigenvalues of the Hessian matrix were calculated when the closest local minimum was reached. The results are listed in Table III. Two observations indicate that the smoothness of the DFT energy landscape is not reproduced by force fields. First, the classical potentials tend to overestimate the average of the largest eigenvalues (first row in Table III) compared to DFT, indicating a rougher PES with high-frequency eigenmodes. The EDIP potential, for example, has a two times higher average of the largest eigenvalue compared to DFT. Second, the eigenvalues of the classical potentials show a higher scatter (second row in Table III), leading to eigenvalues much larger than the average. This is another indication for a rough PES. The Tersoff potential, for example, overestimates the range of the largest eigenvalues by a factor of 13 compared to DFT. The SW potential provides the most accurate results among the force fields with respect to DFT. This is in agreement with its

accurate overall description of low-lying structures. The Lenosky tight binding scheme gives very accurate values for the second derivative of the energy landscape, almost identical to DFT results.

V. CRYSTALLINE DEFECTS AND AMORPHOUS STATES IN BULK SILICON

A. Defects in crystalline silicon

The MHM was used to explore the low-energy region on the PES of bulk silicon. Starting with crystalline cubic diamond structure consisting of 216 Si atoms, 200 000 local minima were found successively for each classical potential during the simulation. For the Lenosky tight binding scheme only 25 000 structures could be found due to limited computer time. Periodic boundary conditions with respect to the ground-state geometry were used to provide the appropriate bulk conditions. The ten energetically lowest configurations of each potential were used as input configurations for geometry relaxations in DFT. Table IV summarizes results for the DFT-relaxed geometries.

The correct ground-state geometry, the well-known diamond structure, is predicted with all the potentials. However, the structures of the first excited state of different force fields do not coincide. For all potentials except the Lenosky force field it is a single fourfold coordinate defect⁵⁹ (FFCD). The Lenosky potential on the other hand predicts a pair of two fourfold coordinated defects⁵⁹ in different regions of the cell as the lowest energy defect structure. The double FFCD is 3.99 eV higher in energy compared to the diamond structure.

The majority of the eight other low-energy geometries in the EDIP potential are structures containing single displaced

TABLE IV. The results of ten configurations of each potential relaxed with DFT. The second column shows the number of stable structures. The following columns show the number of structures which relax to the bulk crystal, to a single FFCD or two FFCDs which are either neighboring (n-FFCD) or distant (d-FFCD).

Method	Stable	Bulk	FFCD	n-FFCD	d-FFCD
EDIP	2	6	4	0	0
Lenosky	10	1	0	2	7
SW	7	1	4	5	0
Tersoff	2	4	6	0	0
LTB	10	1	1	4	4

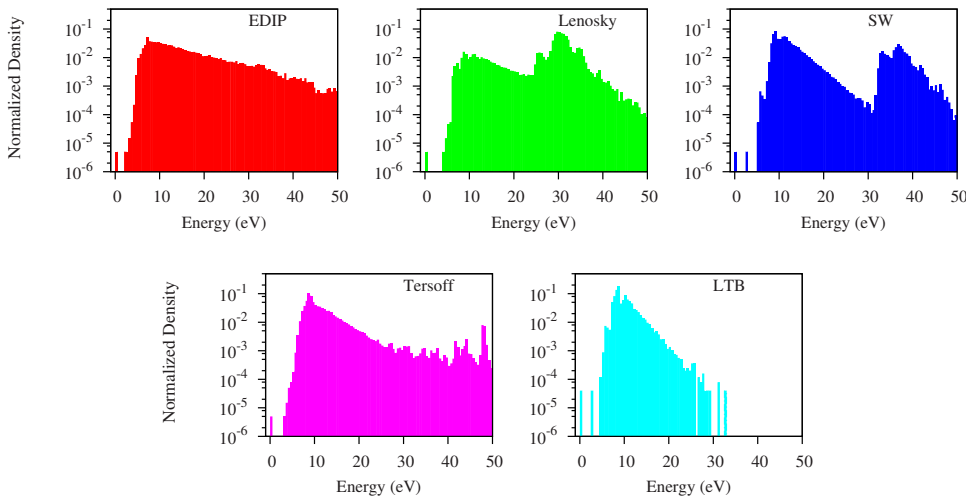


FIG. 9. (Color online) The normalized MH-DOS as represented by a histogram consisting of 100 bins on a logarithmic scale. While 200 000 values were used for the classical potentials only 25 000 could be calculated with the Lenosky tight binding scheme. The energy is shifted such that the ground state has energy 0.

atoms which are either fourfold or fivefold coordinated. Similar structures can be found with the Tersoff potential. All of these excited configurations are unstable in DFT calculations. The Tersoff potential additionally has minima at a variety of slightly distorted FFCDs which are unstable in DFT.

In contrast to the other three force fields, the Lenosky force field always predicts pairs of FFCDs as low-lying energy configurations. They are either neighboring and share a common atom or are distant, i.e., located in different regions of the cell. Even though the single FFCD, which must be the first excited state, is not predicted by the Lenosky force field (the reparametrized Lenosky MEAM does stabilize the single FFCD), all other low-lying energy configurations from the second to ninth excited states are stable in DFT geometry optimization. Nonetheless, the sequence with respect to the energy does not coincide with the sequence in DFT energies. The Stillinger-Weber force field behaves very similarly. Only three structures were found to be unstable, the other five excited states all contain two interacting FFCDs.

The best accuracy can be found with the Lenosky tight binding scheme. All structures exist on the DFT Born-Oppenheimer surface and the energy sequence is correctly described with the exception of the ninth and tenth excited states. They are exchanged in sequence and show an energy difference of 0.02 eV with the Lenosky tight binding scheme and 0.04 eV when calculated with DFT.

B. Configurational density of states of local minima

To describe the overall characteristics of the potential-energy surface we chose the C-DOS which gives the number of configurations per energy interval. The inherent structure approach^{60–62} shows that the C-DOS influences the free energy and hence all thermodynamic quantities. The C-DOS, together with other quantities, was recently used to quantify energy landscapes of solids by Oganov and Valle.⁶³ The correct C-DOS is reproduced by a force field if the energetic ordering is quantitatively correct and if there is a one-to-one mapping between the local minima of the approximate and exact energy landscape. If either condition is not satisfied it is very unlikely that the C-DOS is correctly reproduced.

We approximate this C-DOS by the minima hopping DOS (MH-DOS) which is obtained simply by sampling the low-energy region with the MHM and counting the number of distinct minima found in an energy interval. It has to be stressed that, in the plots we present in this paper, a more or less complete sampling of all minima can only be achieved in a very small interval around the putative global minimum. Only in this small interval of several electron volt we observe in the MH-DOS the expected exponential growth of the number of local minima with respect to the energy of the C-DOS. In our plots we show, however, a much larger energy interval where the number of states is the true number of states multiplied by the probability that a configuration in this energy range will be visited. Since this probability decreases with increasing energy the MH-DOS tends to zero for large energies in all our plots whereas the C-DOS would be orders of magnitude larger. Since the minima hopping method maps out higher energy configurations when the minima hopping run is allowed to continue longer, we cannot only expect a better mapping of the low-energy region but also an extended mapping of higher energies with increasing duration of the simulation. The MH-DOS and C-DOS agree only within the first few bins of the exponential growth region. The lowest energy minima correspond to point defects. The onset of the exponential growth region is due to a growing number of defects (mainly of the FFCD type) which lead continuously to amorphous structures. Some of the potentials also show a second peak at higher energies. This peak is due to amorphous configurations which are related to a sheared crystalline structure. Since we do not relax the simulation cell sheared structures cannot relax.

The reason why we show the MH-DOS over an energy interval which is much larger than the interval within which we can obtain a reliable C-DOS is the following. If there were good agreement between the C-DOS obtained from different force fields the MH-DOS would also agree. As seen from Fig. 9 the MH-DOS obtained from different force fields are drastically different and one can therefore conclude that the C-DOS is also drastically different. The Stillinger-Weber and the Lenosky tight binding show similar features in the low-energy region, e.g., the energy gap between the single FFCD and higher excited states and the spike between 7 and

8 eV. While the EDIP and the Tersoff potentials show only a single major peak around 10 eV, both Lenosky and Stillinger-Weber have a second peak located at about 35 eV which corresponds, as discussed above, to sheared structures. This is due to the fact that for these two potentials the C-DOS of unsheared amorphous structures is much lower than for the other potentials and the MHM starts therefore sampling higher energy regions corresponding to sheared structures. The differences in the C-DOS are responsible for the different speeds with which the putative global minimum is found (see Table II).

VI. DISCUSSION

From our DFT barrier height results it would be tempting to conclude that we have a good overall description of the energy landscape with LDA, PBE, and B3LYP. However, it is known that for interstitial defects in silicon, these methods make approx. 1 eV error in the formation energies.⁶⁴ This error is not entirely systematic—it is a distortion of the potential-energy surface rather than a pure rescaling, but there are systematic trends because DFT is an *ab initio* method and hence based on physical principles. Furthermore many defects have electronic eigenstates within the band gap, which is badly underestimated by LDA and PBE. The occupancy of electronic eigenstates, and hence the total energy, is likely to be mispredicted as they approach the conduction-band edge or tail. These issues and others have been reviewed by Deák *et al.*⁶⁵

Our belief, based on our results, however, is that the exchange-correlation functionals we tried will work rather well for predicting barrier heights in solid-state pure silicon systems in practice. On the other hand, it appears that the distortion of the potential-energy surface, together with occupancy of incorrect electronic eigenstates^{64,65} must cause DFT to predict the wrong local minima and the wrong ordering of local minima in at least some cases. For example, any defect which is surrounded by extremely low barriers might be stable in DFT but unstable in reality or vice versa.

The comparison of Si₈ transition states predicted by DFT and QMC together with the previous studies on stable geometries of semiconductor materials by others justify the use of DFT as a reference method for the larger Si systems considered in the rest of this paper. In case of clusters, all of the force fields failed to predict low-energy structures stable in DFT, while in case of defected diamond structures the Lenosky and SW potentials outperformed the EDIP and the Tersoff, giving very few unphysical local minima, while EDIP and Tersoff mostly had many unphysical minima. This is in agreement with the C-DOS calculations, see Fig. 9, where abundance of minima with energies lower than ≈7.0 eV confirms the existence of many spurious local minima. More precisely, there are two energy gaps in DFT calculations, one between bulk and single FFCD of 2.34 eV, the other between single FFCD and two or more FFCDs of 2.64 eV. These energy gaps are well described by SW and Lenosky tight binding, whereas in EDIP and Tersoff the second gap is occupied by spurious low-energy minima. Although the single FFCD is not stable in the Lenosky potential, it has only a few spurious minima.

A fascinating feature of the silicon energy landscape is the existence of extremely flat regions that can only be assessed by performing very high accuracy calculations. In Fig. 8 we report DFT calculations of a relaxation pathway converged so that maximum force components are less than 0.002 eV/Å against which other methods are then compared. This calculation again shows that SW and the Lenosky force fields are smoother than EDIP and Tersoff with the Lenosky tight binding giving results most similar to DFT. The SW model, additionally, covers too large of an energy range which may be related to its too-stiff phonon energies.²⁷

Even though our results indicate that force fields are problematic for finding local minima reliably, there has been interesting work in this area. The most complex body of work involving finding local minima for silicon systems with a force field is that of Ciobanu and Predescu⁶⁶ and those of Chuang *et al.*^{67,68} They used the original Lenosky force field with global optimization algorithms to find reconstructions for various surfaces such as Si(105), Si(114), and Si(337) that support complex surface reconstructions. In many cases the local minima of the force field were incorrectly ordered but many were stable in DFT, and putative ground-state structures were identified and compared to experiments. Using the reparametrized Lenosky MEAM, local minima were identified for multiple-interstitial clusters.²⁹

VII. CONCLUSIONS

QMC calculations for small clusters have shown that DFT and, in particular, LDA barrier heights are rather accurate for rearrangement processes occurring in silicon systems. This justifies the use of DFT for the estimation of diffusion coefficients and other dynamical properties. Furthermore highly accurate DFT results for structural properties, i.e., local minima of the potential-energy surface, have been reported in numerous publications for different materials as well as for silicon. Therefore, DFT calculations are able to provide very reliable potential-energy surfaces for silicon systems. On the other hand force fields, which are widely used for dynamical simulations in large silicon systems, not always accurately describe the potential-energy surface. In addition, they nearly fail in all cases to describe the energy landscape of silicon clusters. With the exception of the MEAM-based Lenosky force field, all force fields give rise to potential-energy surfaces that are too rough. In an extended crystalline environment most force fields greatly overestimate the configurational density of states because they give rise to many spurious defect structures which do not exist in more accurate schemes. Nonperiodic systems such as clusters present particular problems for classical models, due to the miscoordinated atoms. This is also true at surfaces and grain boundaries. Simulations based on the use of a single force field should therefore be viewed with caution and should be verified by density functional calculations whenever this is feasible. Lenosky tight binding was satisfactory in all of our tests except for the barrier heights. This is presumably valid for other well-developed tight binding schemes as well. We conclude that tight binding is well suited for applications related to geometrical properties of silicon systems, whenever a very high accuracy is not required.

ACKNOWLEDGMENTS

We thank Gustavo Scuseria for interesting discussions. Financial support was provided by the Swiss National Science Foundation. The calculations were done at the Swiss National Supercomputing center (CSCS) in Manno. The work at Cornell University was supported by the National Science Foundation under Grants No. EAR-0703226 and No. EAR-0530813. The research used computational resources provided by the National Energy Research Scientific Com-

puting Center, which is supported by the Office of Science of the U.S. Department of Energy, by Teragrid at the National Center for Supercomputing Applications, which is supported by the National Science Foundation and by the Computational Center for Nanotechnology Innovations, which is supported by the state of New York. An implementation with an identical calling sequence of all the force fields used in this work can be downloaded from www.unibas.ch/comphys/

-
- *stefan.goedecker@unibas.ch; <http://pages.unibas.ch/comphys/comphys/>
- ¹F. Valiquette and N. Mousseau, *Phys. Rev. B* **68**, 125209 (2003).
 - ²A. Broo and A. Holmén, *Chem. Phys.* **211**, 147 (1996).
 - ³S.-F. Wang, J.-K. Feng, C.-C. Sun, P. Liu, Z. Gao, and F.-A. Kong, *Int. J. Quantum Chem.* **81**, 280 (2001).
 - ⁴F. Grein, *J. Chem. Phys.* **130**, 124118 (2009).
 - ⁵A. Fielicke, J. T. Lyon, M. Haertelt, G. Meijer, P. Claes, J. de Haeck, and P. Lievens, *J. Chem. Phys.* **131**, 171105 (2009).
 - ⁶N. X. Wang and A. K. Wilson, *J. Chem. Phys.* **121**, 7632 (2004).
 - ⁷R. G. Parr and Y. Weitao, *Density-Functional Theory of Atoms and Molecules* (Oxford University Press, USA, 1989).
 - ⁸J. P. Perdew, K. Burke, and M. Ernzerhof, *Phys. Rev. Lett.* **77**, 3865 (1996).
 - ⁹D. Ceperley, G. V. Chester, and M. H. Kalos, *Phys. Rev. B* **16**, 3081 (1977).
 - ¹⁰J. B. Anderson, *J. Chem. Phys.* **63**, 1499 (1975).
 - ¹¹D. Ceperley and B. Alder, *Science* **231**, 555 (1986).
 - ¹²C. J. Umrigar, J. Toulouse, C. Filippi, S. Sorella, and R. G. Hennig, *Phys. Rev. Lett.* **98**, 110201 (2007).
 - ¹³J. Toulouse and C. J. Umrigar, *J. Chem. Phys.* **126**, 084102 (2007).
 - ¹⁴J. Toulouse and C. J. Umrigar, *J. Chem. Phys.* **128**, 174101 (2008).
 - ¹⁵W. M. C. Foulkes, L. Mitas, R. J. Needs, and G. Rajagopal, *Rev. Mod. Phys.* **73**, 33 (2001).
 - ¹⁶*Quantum Monte Carlo Methods in Physics and Chemistry*, NATO Advanced Studies Institute, Series C Vol. 525, edited by M. P. Nightingale and C. J. Umrigar (Kluwer, Dordrecht, 1999).
 - ¹⁷B. L. Hammond, J. W. A. Lester, and P. J. Reynolds, *Monte Carlo Methods in Ab Initio Quantum Chemistry* (World Scientific, Singapore, 1994).
 - ¹⁸A. Pedersen, L. Pizzagalli, and H. Jónsson, *J. Phys.: Condens. Matter* **21**, 084210 (2009).
 - ¹⁹H. Balamane, T. Halicioglu, and W. A. Tiller, *Phys. Rev. B* **46**, 2250 (1992).
 - ²⁰J. Samela, K. Nordlunda, J. Keinonen, and V. Popok, *Nucl. Instrum. Methods Phys. Res. B* **255**, 253 (2007).
 - ²¹S. Erkoç and K. Takahashi, *Int. J. Mod. Phys. C* **15**, 403 (2004).
 - ²²L. Nurminen, F. Tavazza, D. P. Landau, A. Kuronen, and K. Kaski, *Phys. Rev. B* **67**, 035405 (2003).
 - ²³H. Hensel, P. Klein, H. M. Urbassek, and T. Frauenheim, *Phys. Rev. B* **53**, 16497 (1996).
 - ²⁴J. Tersoff, *Phys. Rev. B* **39**, 5566 (1989).
 - ²⁵F. H. Stillinger and T. A. Weber, *Phys. Rev. B* **31**, 5262 (1985).
 - ²⁶J. F. Justo, M. Z. Bazant, E. Kaxiras, V. V. Bulatov, and S. Yip, *Phys. Rev. B* **58**, 2539 (1998).
 - ²⁷T. J. Lenosky, B. Sadigh, E. Alonso, V. V. Bulatov, T. D. de la Rubia, J. Kim, A. F. Voter, and J. D. Kress, *Modell. Simul. Mater. Sci. Eng.* **8**, 825 (2000).
 - ²⁸M. I. Baskes, *Phys. Rev. Lett.* **59**, 2666 (1987).
 - ²⁹Y. A. Du, T. J. Lenosky, R. G. Hennig, S. Goedecker, and J. W. Wilkins (unpublished).
 - ³⁰H. Park and J. W. Wilkins, *Phys. Rev. B* **79**, 241203(R) (2009).
 - ³¹T. J. Lenosky, J. D. Kress, I. Kwon, A. F. Voter, B. Edwards, D. F. Richards, S. Yang, and J. B. Adams, *Phys. Rev. B* **55**, 1528 (1997).
 - ³²P. J. Stephens, F. J. Devlin, C. F. Chabalowski, and M. J. Frisch, *J. Phys. Chem.* **98**, 11623 (1994).
 - ³³L. Genovese, A. Neelov, S. Goedecker, T. Deutsch, S. A. Ghasemi, O. Zilberberg, A. Bergman, M. Rayson, and R. Schneider, *J. Chem. Phys.* **129**, 014109 (2008).
 - ³⁴S. Goedecker, M. Teter, and J. Hutter, *Phys. Rev. B* **54**, 1703 (1996).
 - ³⁵C. Hartwigsen, S. Goedecker, and J. Hutter, *Phys. Rev. B* **58**, 3641 (1998).
 - ³⁶J. R. Trail and R. J. Needs, *J. Chem. Phys.* **122**, 174109 (2005).
 - ³⁷M. W. Schmidt *et al.*, *J. Comput. Chem.* **14**, 1347 (1993).
 - ³⁸*Theory and Applications of Computational Chemistry: The First Forty Years*, edited by C. E. Dykstra, G. Frenking, K. S. Kim, and G. E. Scuseria (Elsevier, Amsterdam, 2005), pp. 1167–1189.
 - ³⁹G. H. Vineyard, *J. Phys. Chem. Solids* **3**, 121 (1957).
 - ⁴⁰L. Mitas, J. C. Grossman, I. Stich, and J. Tobik, *Phys. Rev. Lett.* **84**, 1479 (2000).
 - ⁴¹D. K. Yu, R. Q. Zhang, and S. T. Lee, *Phys. Rev. B* **65**, 245417 (2002).
 - ⁴²L. Tsetseris, G. Hadjisavvas, and S. T. Pantelides, *Phys. Rev. B* **76**, 045330 (2007).
 - ⁴³Y. Kanai, X. Wang, A. Selloni, and R. Car, *J. Chem. Phys.* **125**, 234104 (2006).
 - ⁴⁴J. C. Grossman and L. Mitas, *Phys. Rev. Lett.* **79**, 4353 (1997).
 - ⁴⁵D. M. Ceperley and B. J. Alder, *J. Chem. Phys.* **81**, 5833 (1984).
 - ⁴⁶D. L. Diedrich and J. B. Anderson, *Science* **258**, 786 (1992).
 - ⁴⁷W. Hellmann, R. G. Hennig, S. Goedecker, C. J. Umrigar, B. Delley, and T. Lenosky, *Phys. Rev. B* **75**, 085411 (2007).
 - ⁴⁸A. Heyden, A. T. Bell, and F. J. Keil, *J. Chem. Phys.* **123**, 224101 (2005).
 - ⁴⁹Y. Zhao, N. González-García, and D. G. Truhlar, *J. Phys. Chem. A* **109**, 2012 (2005).
 - ⁵⁰S. Andersson and M. Grüning, *J. Phys. Chem. A* **108**, 7621

- (2004).
- ⁵¹M. Grüning, O. V. Gritsenko, and E. J. Baerends, *J. Phys. Chem. A* **108**, 4459 (2004).
- ⁵²S. Patchkovskii and T. Ziegler, *J. Chem. Phys.* **116**, 7806 (2002).
- ⁵³J. P. Perdew and A. Zunger, *Phys. Rev. B* **23**, 5048 (1981).
- ⁵⁴A. J. Cohen, P. Mori-Sánchez, and W. Yang, *Science* **321**, 792 (2008).
- ⁵⁵S. Goedecker, *J. Chem. Phys.* **120**, 9911 (2004).
- ⁵⁶S. E. Schönborn, S. Goedecker, S. Roy, and A. R. Oganov, *J. Chem. Phys.* **130**, 144108 (2009).
- ⁵⁷D. J. Wales, *Energy Landscapes* (Cambridge University Press, Cambridge, 2003).
- ⁵⁸R. S. Berry, N. Elmaci, J. P. Rose, and B. Vekhter, *Proc. Natl. Acad. Sci. U.S.A.* **94**, 9520 (1997).
- ⁵⁹S. Goedecker, T. Deutsch, and L. Billard, *Phys. Rev. Lett.* **88**, 235501 (2002).
- ⁶⁰F. H. Stillinger and T. A. Weber, *Phys. Rev. A* **25**, 978 (1982).
- ⁶¹F. H. Stillinger and T. A. Weber, *Science* **225**, 983 (1984).
- ⁶²F. H. Stillinger, *Science* **267**, 1935 (1995).
- ⁶³A. R. Oganov and M. Valle, *J. Chem. Phys.* **130**, 104504 (2009).
- ⁶⁴E. R. Batista, J. Heyd, R. G. Hennig, B. P. Uberuaga, R. L. Martin, G. E. Scuseria, C. J. Umrigar, and J. W. Wilkins, *Phys. Rev. B* **74**, 121102(R) (2006).
- ⁶⁵P. Deák, B. Aradia, T. Frauenheima, and A. Galib, *Mater. Sci. Eng., B* **154-155**, 187 (2008).
- ⁶⁶C. V. Ciobanu and C. Predescu, *Phys. Rev. B* **70**, 085321 (2004).
- ⁶⁷F. C. Chuang, C. V. Ciobanu, C. Z. Wang, and K.-M. Ho, *J. Appl. Phys.* **98**, 073507 (2005).
- ⁶⁸F. C. Chuang, C. V. Ciobanu, C. Predescu, C. Z. Wang, and K. Ho, *Surf. Sci.* **578**, 183 (2005).